Journal of Hydrology 404 (2011) 186–197

Contents lists available at ScienceDirect

Journal of Hydrology

journal homepage: www.elsevier.com/locate/jhydrol

# Spatio-temporal patterns of soil water storage under dryland agriculture at the watershed scale

Hesham M. Ibrahim [a,*], David R. Huggins [b]

[a] Department of Crop and Soil Sciences, Washington State University, Pullman, WA 99164, United States
[b] USDA-ARS, Land Management and Water Conservation Research Unit, Washington State University, Pullman, WA 99164, United States

ARTICLE INFO

*Article history:*
Received 19 August 2010
Received in revised form 25 January 2011
Accepted 20 April 2011
Available online 4 May 2011
This manuscript was handled by P. Baveye, Editor-in-Chief

*Keywords:*
Soil water variability
Empirical orthogonal function
Terrain and soil variability
Field patterns of water storage

SUMMARY

Spatio-temporal patterns of soil water are major determinants of crop yield potential in dryland agriculture and can serve as the basis for delineating precision management zones. Soil water patterns can vary significantly due to differences in seasonal precipitation, soil properties and topographic features. In this study we used empirical orthogonal function (EOF) analysis to characterize the spatial variability of soil water at the Washington State University Cook Agronomy Farm (CAF) near Pullman, WA. During the period 1999–2006, the CAF was divided into three roughly equal blocks (A, B, and C), and soil water at 0.3 m intervals to a depth of 1.5 m measured gravimetrically at approximately one third of the 369 geo-referenced points on the 37-ha watershed. These data were combined with terrain attributes, soil bulk density and apparent soil conductivity ($EC_a$). The first EOF generated from the three blocks explained 73–76% of the soil water variability. Field patterns of soil water based on EOF interpolation varied between wet and dry conditions during spring and fall seasons. Under wet conditions, elevation and wetness index were the dominant factors regulating the spatial patterns of soil water. As soil dries out during summer and fall, soil properties ($EC_a$ and bulk density) become more important in explaining the spatial patterns of soil water. The EOFs generated from block B, which represents average topographic and soil properties, provided better estimates of soil water over the entire watershed with larger Nash–Sutcliffe Coefficient of Efficiency (NSCE) values, especially when the first two EOFs were retained. Including more than the first two EOFs did not significantly increase the NSCE of soil water estimate. The EOF interpolation method to estimate soil water variability worked slightly better during spring than during fall, with average NSCE values of 0.23 and 0.20, respectively. The predictable patterns of stored soil water in the spring could serve as the basis for delineating precision management zones as yield potential is largely driven by water availability. The EOF-based method has the advantage of estimating the soil water variability based on soil water data from several measurement times, whereas in regression methods only soil water measurement at a single time are used. The EOF-based method can also be used to estimate soil water at any time other than measurement times, assuming the average soil water of the watershed is known at that time.



## 1. Introduction

Many hydrological processes are regulated by spatio-temporal variability of soil water including surface and subsurface flow, erosion, and chemical transport. In agriculture, soil water variation also affects evapotranspiration (Wood, 1997), and plant growth (Jaynes et al., 2003; Green and Erskine, 2004). Characterizing spatio-temporal variability associated with soil water is fundamental to understanding and modeling the above processes, particularly as relationships among various biophysical processes and soil water are complex and often nonlinear. For example, Wood (1997) showed that the use of spatially-averaged soil water in lumped-parameter models led to under-estimates of evapotranspiration during high demand periods, and over-estimates during low demand periods. Western et al. (1999a) showed the impact of soil water variation on stream discharge in response to rainfall events, and illustrated the importance of accurate representation of soil water spatial patterns for accurate estimation of runoff. In dryland agriculture, crop yield potential is often determined by water availability and understanding field-scale variations in stored water is critical to the application of precision farming practices (Fiez et al., 1995; Pan et al., 2007).

Soil water is often assessed using ground-based measurements either directly using gravimetric methods, or indirectly using neutron moderation or time-domain reflectometry (TDR).

* Corresponding author. Permanent address: Department of Soils and Water, Suez Canal University, Ismailia 41522, Egypt. Tel.: +1 509 335 3653; fax: +1 509 335 8674.
*E-mail address:* habdou_1@hotmail.com (H.M. Ibrahim).

0022-1694/$ - see front matter © 2011 Elsevier B.V. All rights reserved.
doi:10.1016/j.jhydrol.2011.04.029

Ground-based measurements, however, are equipment intensive, time consuming, and expensive. In addition, the volume of soil measured using these techniques is relatively small, and only an average measure of soil water over an aerial extent is usually obtained. As a result, the analysis of spatial correlation of soil water among points is often limited by the small number of highly variable point measurements (Western and Grayson, 1998; Western et al., 1998). Remote sensing using both passive and active microwave can detect near-surface soil water at larger scales (Jackson and Le Vine, 1996; Ulaby et al., 1996; Pietroniro and Prowse, 2002). Remote sensing data, however, often require downscaling methodology to assess soil water variability at scales that are relevant to hydrologic processes (Hu et al., 1998; Kim and Barros, 2002). Remote sensing waves also interact with vegetative cover of the land and with surface roughness (Jackson and Le Vine, 1996) and are limited to quantification of the soil surface, whereas many hydrological and agricultural applications require knowledge of soil water variability over the entire soil profile root zone (Wilson et al., 2003).

Several methodologies have been used to overcome the problems associated with direct and indirect methods to assess soil water variability. These methods vary from statistical approaches and regression analyses to the application of physically-based models. Various kriging methods have been used to interpolate both TDR measurements of soil water (Bardossy and Lehmann, 1998), and remotely sensed soil water data (Thattai and Islam, 2000). Western et al. (1998) analyzed the spatial correlation structure of soil water patterns at the Tarrawarra catchment. They reported the development of a seasonal geostatistical structure with correlation lengths between 35 and 50 m during the wet winter conditions, and longer correlation lengths between 50 and 60 m during the dry summer conditions. The observed seasonal variations in soil water patterns were hypothesized to result from differences in soil water redistribution via lateral flow mechanisms that occurred during wet versus dry periods (Western et al., 1998). Similar findings were reported by Florinsky et al. (2002) who concluded that such dynamic behavior makes interpolation difficult. Wilson et al. (2005) used a dynamic multiple linear regression model to enhance the characterization of the spatial patterns of soil water. The model incorporates a weighted combination of topographic attributes, soil and vegetation data, and a stochastic component to account for unrepresented soil water variation. The weights were based on the relationships between average soil water and the spatial patterns of the attributes.

Several factors dominate the complex dynamics of soil water including, soil properties (Kim and Stricker, 1996), topography (Crave and Gascuel-Odoux, 1997; Yoo et al., 1998; Yoo and Kim, 2004), land use and vegetation (Yoo et al., 2001; Hupet and Vanclooster, 2002; Williams et al., 2003), and precipitation (Yoo et al., 2001; Cosh et al., 2004). Among all these factors, topography has received greater attention due to the wide availability of topographic data and the simple methods available to identify and quantify spatial variations of topographic attributes. Nevertheless, patterns of soil water are rarely organized in space to the same degree as topographic attributes, and are also more temporally dynamic (Burt and Butcher, 1985). Topographic attributes often play a more important role in controlling soil water dynamics during wet periods, which promote overland and subsurface lateral flow (Wilson et al., 2005). Nyberg (1996) examined the spatial variability of soil water for a 6300 $m^2$ covered catchment in Sweden. He calculated four different topographic indices and found that water content was positively correlated with the size of the upslope drainage area indicating that topography was a major regulator of soil water variation. The size of the upslope draining area is called the specific contributing area (Famigliett et al., 1998). Specific contributing areas affect soil water patterns by influencing the amount of surface and subsurface water flow, as the size of the area increases so does the potential for greater wetness at lower elevations (Famigliett et al., 1998). Topographic regulation of soil water is often less during extreme wet and dry conditions (Western et al., 1999b). Under these conditions, soil water is likely to be more spatially uniform and regulated by characteristics of soil porosity and water retention (Western et al., 2003).

Western et al. (1999b) analyzed TDR point measurements of surface soil water (top 0.3 m) at 13 different times from September, 1995 to November, 1996 at the Tarrawarra catchment. They found consistent spatial patterns of soil water during wet periods, whereas very little spatial organization of soil water was observed during dry periods. Based on correlation analysis they found that the specific contributing area expressed as $\ln(a)$, where $a$ is the specific upslope area, was the best predictor of the soil water pattern during wet conditions. The angle of the surface slope ($\beta$) was of lesser importance in the correlation analysis. These two variables represent the Wetness Index, $\ln(a/\tan\beta)$, defined as the natural log of the ratio between the surface area ($a$) draining through a unit length and the local slope ($\tan\beta$), used in the TOPMODEL (Beven and Kirkby, 1979). Western et al., 1999b found that the specific contributing area was associated with surface and subsurface lateral flow, whereas the potential radiation index, defined as the ratio of the potential solar radiation on a sloping plane to the potential solar radiation on a horizontal plane, was associated with vertical flow and evapotranspiration, and was a better predictor for soil water during dry conditions. The combination of these factors accounted for 61% and 22% of soil water variability in the Tarrawarra catchment during wet and dry periods, respectively.

The complex spatio-temporal dynamics of soil water have also been examined using empirical orthogonal function (EOF) analysis. Introduced in the atmospheric sciences, EOF is now widely used in other fields (Preisendorfer, 1988). Kim and Barros (2002) used EOF analysis to assess the spatial patterns of soil water from large scale remote sensing images obtained during the Southern Great Plains (SGP97) experiment. They found at high water contents, close to or above field capacity, that soil water variability was greatly influenced by topographic attributes. As the soil started to dry during inter-storm periods, topographic effects diminished as lateral water flow became less important and vertical flow more important. As a result the spatial variability of soil water became increasingly associated with soil properties (especially percent sand), and with evapotranspiration processes as soil drying continued (Kim and Barros, 2002). Perry and Niemann (2007) reported that EOF analysis of soil water variability at the Tarrawarra catchment in Australia revealed two distinct spatial patterns. The first spatial pattern, which explained 55% of soil water variation, was correlated with topographic attributes such as the natural log of the specific contributing area, an indication that lateral redistribution of water was an important contributing process. The second spatial pattern explained 9% of the spatial variation and was correlated with aspect, indicating an association of spatial pattern with evapotraspiration (Perry and Niemann, 2007).

In the Palouse region of the Inland Pacific Northwest, landscape and soil attributes produce complex spatial and temporal variations with respect to microclimate and water storage and movement (Busacca and Montgomery, 1992). Soil water recharge occurs during winter months and peaks during the early spring, prior to significant crop evapotranspiration. Studies with bromide and dye tracers indicate that extensive lateral and vertical chemical movement can occur in certain landscape positions (Mallawatantri et al., 1996). Eroded soils exhibit low water holding capacity and shallower effective rooting depths, which limit water storage, use and yield potential (Pan and Hopkins, 1991; Fiez et al., 1995). Summers are typified by low precipitation and high evapotranspiration that results in soil water depletion and dry soil water

conditions following crop harvest. In this research we use EOF analysis across a 37 ha field at the Washington State University Cook Agronomy Farm (CAF) near Pullman, WA to characterize the spatial variability of soil water at two time periods: (1) maximum recharge in the spring, prior to planting; and (2) following soil water depletion by the crop (after harvest) and prior to the period of soil water recharge when the driest soil water conditions occur. Specific objectives are to: (1) examine spatial patterns of soil water variability using EOF analysis; (2) correlate the spatial patterns of soil water to topographic and soil properties; and (3) interpolate EOF patterns among different parts of the field to estimate soil water at unmeasured locations and unobserved times.

## 2. Materials and methods

### 2.1. Field site and data description

The CAF is a research facility located 10 km to the NE of Pullman, Washington (46°47′N, 117°5′W) that includes direct-seed cropping systems and precision agriculture research. Our research was conducted on a 37-ha field located within the CAF, which is divided into three roughly equal blocks (A, B, and C) that represent three phases of a 3 year rotation that was initiated in 2001 consisting of winter wheat (*Triticum aestivum* L.)-X-spring wheat, where X represents one of six alternative crops (Fig. 1a). In 1998, using a systematic nonaligned grid, a total of 369 geo-referenced locations were identified over the 37-ha field (Fig. 1a). Intensive ground-based measurements of soil water were conducted at the 369 geo-referenced locations from 1999 to 2006. Soil cores (5.37 cm i.d. and 3 cm length) were collected during the fall and spring at 0.3 m depth increments to 1.5 m on about one third of the geo-referenced locations, and soil water was determined gravimetrically. During 1999 and 2000 the entire field was planted to hard red spring wheat (1999) and spring barley (*Hordeum vulgare* L.) (2000), and soil water was sampled within horizontal (1999) and vertical (2000) field areas encompassing locations from all three blocks (Fig. 1a). During the period 2001–2006, crop rotations were initiated and soil water was only sampled at georeferenced locations in the block (A, B, or C) containing spring wheat. Therefore, each entire block (A, B or C) was sampled two times during the study period, while portions of every block were sampled in 1999 and 2000.

A comprehensive database of topographic attributes, soil properties, and crop data has been collected for the CAF and was used for this research (Uberuaga, 2004). A digital elevation model (DEM) of the 37-ha field was developed using a survey grade differential global positioning system (DGPS; Trimble RTK 4400) comprised of a base station and a rover unit where elevation data with corresponding Easting and Northing values were collected in the fall of 1999. The projection used was Universal Transverse Mercator (UTM) with World Geodetic System (WGS) 1984 zone 11 N datum. When operating with at least four satellites, the Trimble unit is capable of gathering measurements in the vertical and horizontal plane with an accuracy of 0.02 m every second (Trimble Navigation, 2001). The DGPS survey resulted in 30,440 Easting and Northing values with corresponding elevation data for the 37-ha field, an average of one point for every 12.16 $m^2$. The maximum predicted horizontal error was 2.74 cm with a mean of 1.09 cm, while the maximum predicted vertical error was 4.56 cm with a mean of 1.74 cm. A series of increasing raster cell size DEMs, 1-m, 2-m, 5-m, 10-m, 15-m, 20-m, 25-m, and 30-m, were created using a Local Polynomial Interpolation (LPI) with 30% global and 70% local polynomial influence (ESRI ArcGIS v. 8.2). Fig. 1b shows the 10-m DEM generated for the CAF. Terrain attributes derived from the resulting DEMs were slope (degrees), plan curvature (radians 100 $m^{-1}$), profile curvature (radians 100 $m^{-1}$), tangential curvature (radians 100 $m^{-1}$), flow accumulation (No. of $x$-$m^2$ cells, where $x$ is the raster cell size), flow direction, specific catchment area (m), wetness index and aspect (ESRI ArcGIS v. 8.2). The terrain attributes calculated from the 5-m, 10-m, and 15-m raster were used in this study.

A kinematic survey of apparent electrical conductivity ($EC_a$) was conducted using an EM38 (Geonics Limited, 2000) operated in the vertical dipole mode and coupled with a Trimble Ag 132

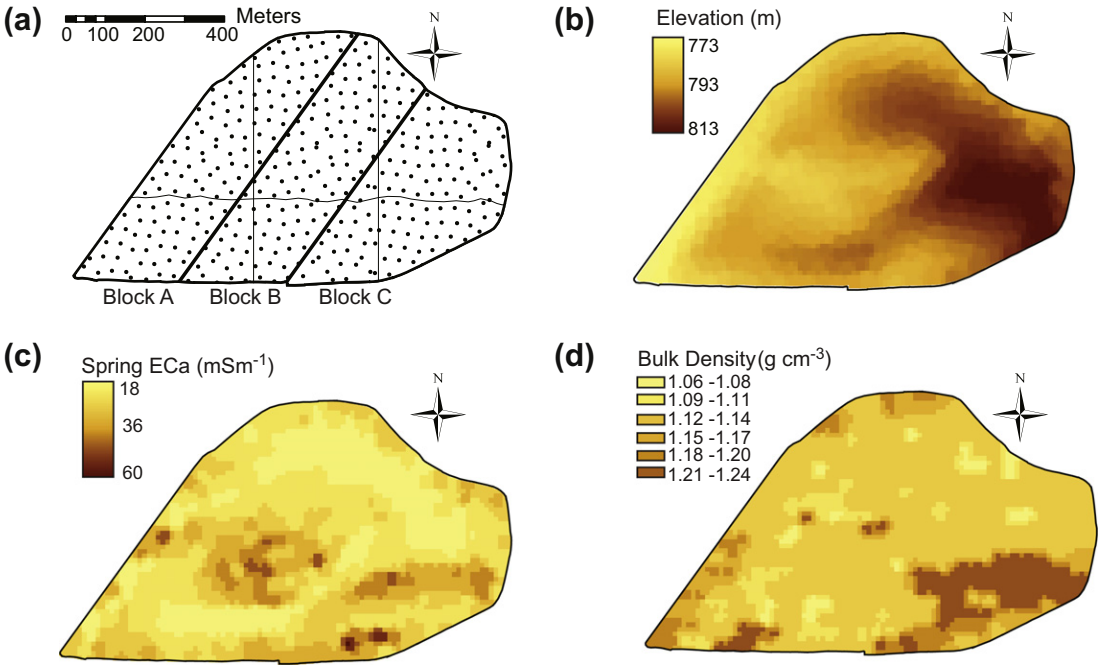


**Fig. 1.** Locations of the 369-georeferenced measurement points, the bottom horizontal and the middle vertical areas show the sampling areas during the years 1999 and 2000, respectively, and the bold diagonal lines show the separation of the three blocks of the WSU Cook Agronomy Farm (CAF) (a); a 10-m Digital Elevation Model of the CAF (b); an interpolated map showing the electromagnetic readings of soil salinity ($EC_a$) in the CAF during spring 2000 (c); and an interpolated map showing bulk density values in the top 0.3 m of the CAF (d).

Differential GPS (DGPS), UTM WGS84 zone 11 N. When operated in the vertical dipole mode, the effective measurement depth is about 1.5 m (Sudduth et al., 2001). Readings from the EM38 were coupled with location data provided by the DGPS every second using the HGIS software package (StarPal, 1997). The $EC_a$ survey was conducted twice: March 25, 2000, just prior to planting spring barley, and on September 14, 2000, following spring barley harvest. The output text files were imported into Geostatistical Software Library (GSLIB), (Deutsch and Journel, 1992) where interpolation of both the spring and fall $EC_a$ data was accomplished using ordinary kriging (Fig. 1c). Bulk density samples were collected at 0.3 m to a depth of 1.5 m at 29 locations. The locations were distributed over the three blocks to ensure that all soil types found in the 37-ha field were represented (Fig. 1d). At each location of the 369 georeferenced locations, gravimetric soil water were transformed into volumetric soil water using soil bulk density and were summed over the profile depth to provide total volumetric water content for the surface 1.5 m of the soil profile.

### 2.2. EOF analysis

A detailed description of the mathematical treatment and notation of the EOF analysis is provided by Preisendorfer, 1988. Fig. 2 shows a schematic diagram of the EOF analysis and the procedures for soil water estimation at the CAF. The spatial anomalies were calculated by subtracting the field-average soil profile water at a specific observation time from the soil profile water at the sample location. Mathematically this can be represented for a location $i$ and at a sampling time $t$ as:

$$x_i(t) = s_i(t) - \frac{1}{m}\sum_{j=1}^{m} s_j(t) \tag{1}$$

where $x_i(t)$ is the spatial anomaly at location $i$ and time $t$, $s_i(t)$ is the soil water value, $j$ is an index number used to sum over the total number of locations ($m$). Spatial anomalies are used in the analysis to minimize temporal variability (Perry and Niemann, 2007). The analysis starts by organizing the spatial anomalies of soil water values at different observation times into a $(m \times n)$ matrix $X$ (Fig. 2, step 1), where $m$ is the number of locations and $n$ is the number of observation times. The spatial anomaly matrix $X$ is used to generate the spatial covariance matrix $Z$ $(n \times n)$ according to the relation (Fig. 2, step 2):

$$Z = \frac{1}{m}X^T X \tag{2}$$

where the superscript $T$ indicates the transpose of the matrix. Since the matrix $Z$ is square and symmetrical, we can use eigen-analysis to diagonalize the matrix (i.e. find its eigenvectors and eigenvalues), the result of this analysis is two more matrices that satisfy the relation (Fig. 2, step 3):

$$ZE = LE \tag{3}$$

where $E$ is a $(n \times n)$ matrix with its columns representing the eigenvectors of matrix $Z$, and $L$ is a $(n \times n)$ matrix containing the associated eigenvalues along the diagonal. The new diagonalized matrix $Z$ is a transformation representing a rotation of the original coordinate axes into a new set of axes in multidimensional space, weighted by the eigenvectors contained in the $E$ matrix. Each sampling time is represented by one dimension and each new axis is set to be orthogonal to all next axes. The amount of variance in the original spatial anomaly that is explained by each new rotated axis is shown by the associated eigenvalues (i.e. the diagonal values of the $L$ matrix).

The projection of the spatial anomaly onto the new rotated axes will produce a new matrix, which describes the spatial anomaly in terms of the newly rotated axes. This is represented mathematically by:

$$F = XE \tag{4}$$

where $F$ is the new projected matrix with dimensions $(m \times n)$. Each column of $F$ is called a spatial pattern (EOF), and represents the new variables for each location based on the new rotated axis. Each column of $E$ is called an expansion coefficient (EC), which are a time series indicating the importance of the spatial patterns at different observation times.

EOF analysis produces $n$ number of EOF/EC pairs. The importance of each pair (i.e. the amount of variance they explain) is expressed in the associated eigenvalues, with the first pair being the most important followed by the second, and so on. The summation of all the eigenvalues explains the total amount of variance found in the original spatial anomaly (Perry and Niemann, 2007). To determine the number of EOFs to retain, we examined whether the spatial patterns generated by the different EOFs were statistically significant for blocks A, B, and C using the approach detailed by North et al. (1982). The test can be written in the form (Fig. 2, step 4):

$$\delta\lambda_j = \lambda_j(2/m)^{1/2} \tag{5}$$

where $\lambda_j$ is the $j$th eigenvalue associated the $j$th EOF/EC pair, and $m$ is the number of independent sampling locations. The confidence interval is then determined as $\lambda_j \pm \delta\lambda_j$. North et al. (1982) suggested that if the sampling error (i.e. the confidence interval) of any eigenvalue is smaller than the spacing between this eigenvalue and the next one (i.e. no overlapping between the confidence intervals), then the associated EOF is statistically different. The generated EOFs from the three blocks were interpolated to represent the entire field using a stepwise multiple linear regression procedure (SMLR) against topographic and soil attributes (Fig. 2, step 5). Linear correlations between the generated and interpolated EOFs were examined for the three blocks A, B, and C (Fig. 2, step 6).

The relationship between the spatial patterns of soil water and topographic and soil properties was analyzed using correlation coefficient analysis. Correlation coefficients between the EOFs generated from the three blocks and soil and topographic properties were evaluated, and weighted correlations were determined by weighting the correlation coefficients by the amount of variance explained by each EOF (Fig. 2, step 7).

Both the spatial patterns EOF and the expansion coefficients EC were used to reconstruct the original spatial anomaly using the relation:

$$X = FE^T \tag{6}$$

Depending on the number of EOFs that were retained from the analysis, we used Eq. (6) to estimate soil water at any location of interest as follow:

$$\hat{s}_{ij} = \bar{s}_j + \sum_{k=1}^{d} \hat{F}_{ik}\hat{E}^T_{kj} \tag{7}$$

where $\hat{s}_{ij}$ is the estimated soil water at location $i$ and time $j$, $\bar{s}_j$ is the average soil water at time $j$, $\hat{F}_{ik}$ is the estimated value of $k$th order EOF at location $i$, $d$ is the number of EOFs retained in the analysis, and $\hat{E}^T_{kj}$ is the transpose of the estimated $k$th order EC associated with each EOF.

Eq. (7) was used to estimate soil water at any time of interest, other than measurement times, using the interpolated spatial pattern (EOFs), which are time invariant (Fig. 2, step 8). However, an estimation of the EC values at these times needs to be determined. Since the spatial average soil water was known at all measurement times, a plot showing EC values at different spatial average soil water would provide a simple methodology to estimate the EC

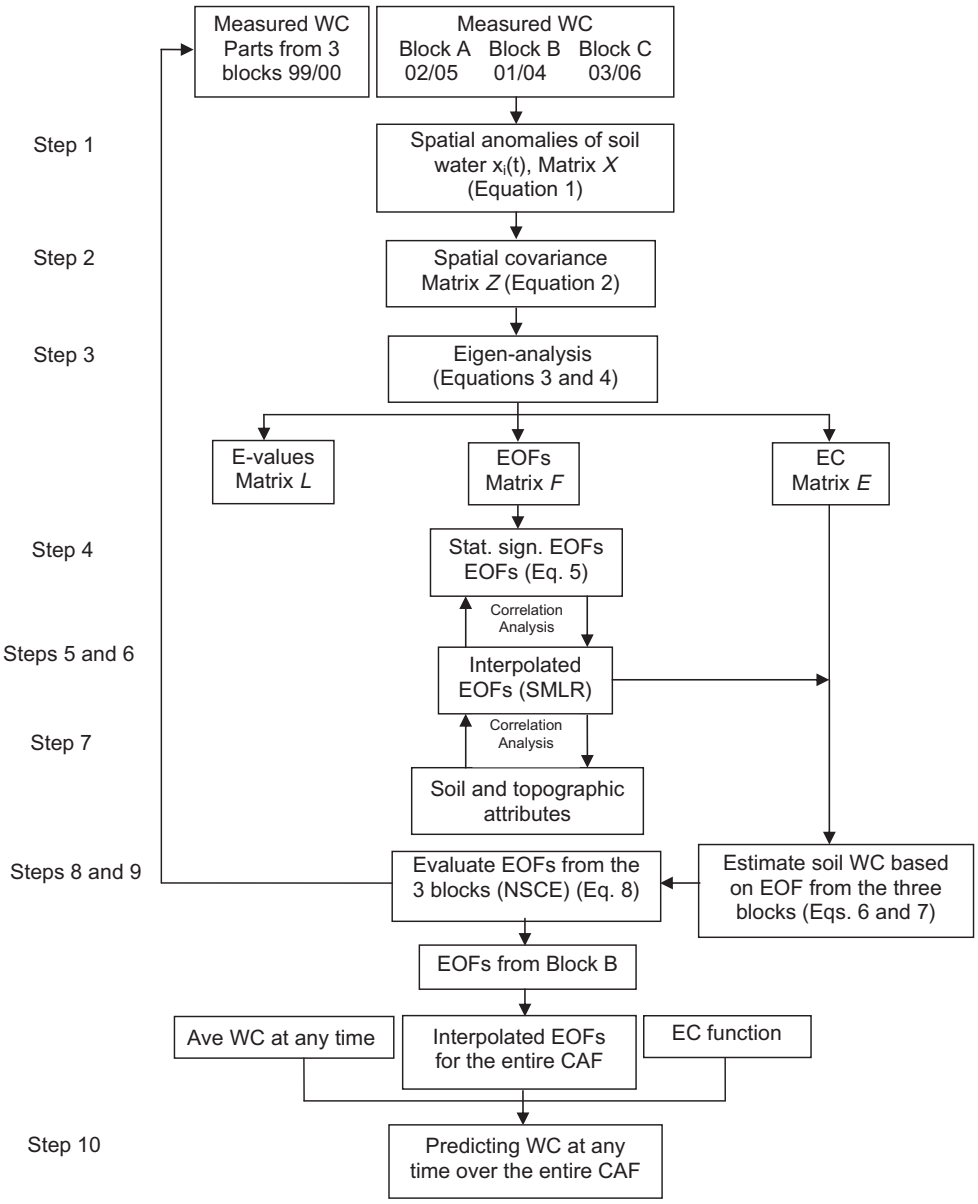


**Fig. 2.** Schematic diagram of the EOF analysis and the procedures for soil water estimation at the CAF. Measured water content (WC) were summed over the top 5 feet of the soil profile during fall and spring of 2001/2004 (block B), 2002/2005 (block A), 2003/2006 (block C), and in parts of all three blocks during fall and spring of 1999/2000.

values at other times. We used this relationship to estimate an EC value at any measurement time using the known average soil water at that time.

Average soil water in the surface 1.5 m of the profile was estimated using the interpolated EOF and the observed EC values. Soil water during spring and fall of the years 2001–2006 were estimated based on statistically significant EOF/EC pairs from the three blocks. To assess the accuracy of the soil water content estimates as compared to measured soil water content, we used the Nash–Sutcliffe Coefficient of Efficiency (NSCE) described as (Nash and Sutcliffe, 1970):

$$\mathrm{NSCE} = \frac{\sum(s_{ij} - \bar{s}_j)^2 - \sum(s_{ij} - \hat{s}_{ij})^2}{\sum(s_{ij} - \bar{s}_j)^2} \quad (8)$$

where $s_{ij}$ is the measured soil water, $\bar{s}_j$ is the average soil water at time $j$, and $\hat{s}_{ij}$ is the estimated soil water at location $i$ and time $j$. The ability of the interpolated EOFs from the three blocks A, B, and C to accurately estimate average soil water at each block was evaluated (Fig. 2, step 9). We examined the performance of the EOF interpolation method, in estimating soil water, when using the first EOF/EC pair, and when additional EOF/EC pairs were included in the estimation. The estimation of soil water over the entire CAF was repeated using an increased number of EOF/EC pairs until all generated EOF/EC pairs were included, and NSCE values of the soil water estimates were determined and compared. The interpolated EOFs from the three blocks were used to estimate soil water content over the entire CAF during the years 1999–2000. These 2 years were selected since soil water measurements were performed on parts of all three blocks in these years. EOFs from the block that provided the best performance were used to estimate average soil water for the entire CAF (Fig. 2, step 10).

## 3. Results and discussions

### 3.1. EOF analysis of the spatial anomalies

Analysis of the spatial anomalies for soil water produced four EOF/EC pairs at each of the three blocks. The amount of variance

**Table 1**
Percentage of variance explained by each EOF generated from the three blocks of the CAF and correlation coefficients between the generated EOFs and the interpolated EOFs based on the SMLR with soil and topographic attributes.

| CAF | Variance explained (%) | | | | Correlation coefficients | | | |
|---|---|---|---|---|---|---|---|---|
| | EOF1 | EOF2 | EOF3 | EOF4 | EOF1 | EOF2 | EOF3 | EOF4 |
| Block A | 0.74 | 0.18 | 0.05 | 0.03 | 0.73 | 0.45 | 0.15 | 0.20 |
| Block B | 0.73 | 0.14 | 0.09 | 0.04 | 0.79 | 0.54 | 0.21 | 0.26 |
| Block C | 0.76 | 0.19 | 0.03 | 0.02 | 0.74 | 0.63 | 0.10 | 0.20 |

explained by the first EOF in the three blocks as determined by the associated eigenvalues, ranged from 73% to 76% (Table 1). More variability was found among the three blocks with regard to the second and third EOF patterns. For example, EOF 2 explained 14% and 19%, and EOF 3 explained 9% and 3% of the variance in the B and C blocks, respectively (Table 1). EOF 4 explained only about 2–4% of the soil water variability in the three blocks. The fact that one single EOF can explain this large amount of variance indicates the possibility that similar or complementary processes regulate the spatial pattern of soil water variation within the CAF. It also suggests that much of the spatial pattern of soil water variability is insensitive to time. Similar findings were reported by Jawson and Niemann, 2007, who used the SGP97 dataset to examine the possibility of characterizing the spatio-temporal variability of soil water at larger scales (~10,000 km$^2$) by identifying a small number of spatial structures related to local soil properties and topographic attributes. They found that a single EOF explained 61% of the spatial variability in soil water, and that it was mostly correlated with soil properties such as percent sand and clay. In addition, as crop yield potential under dryland conditions is driven by water availability, similar spatial patterns of soil water from season-to-season could enable the delineation of precision management zones.

EOF analysis produced positive EC1 values at the three blocks, with larger values during the spring and smaller values during the fall (data not shown). EC2 gave positive and negative values and varied among the three blocks. In blocks B and C, EC2 values showed positive large values during fall and negative lower values during spring. In contrast, block A showed large EC2 values during spring and negative lower values during fall. The overall relationship between the generated EC1 and EC2 from the three blocks and the average water content at the different measurement times was nonlinear with many scattered points, and was best approximated by a second degree polynomial. The fitted curve showed maximum EC1 values at moderate average soil water ($r^2$ = 0.62), and minimum EC2 values at moderate to large average soil water ($r^2$ = 0.2).

Only the first two EOF/EC pairs were found to be statistically significant in blocks B and C. For block A, all four EOF/EC pairs were found to be significant. Correlation analysis between the generated and interpolated EOFs showed that linear correlation coefficients between the generated and interpolated EOFs were, in general,

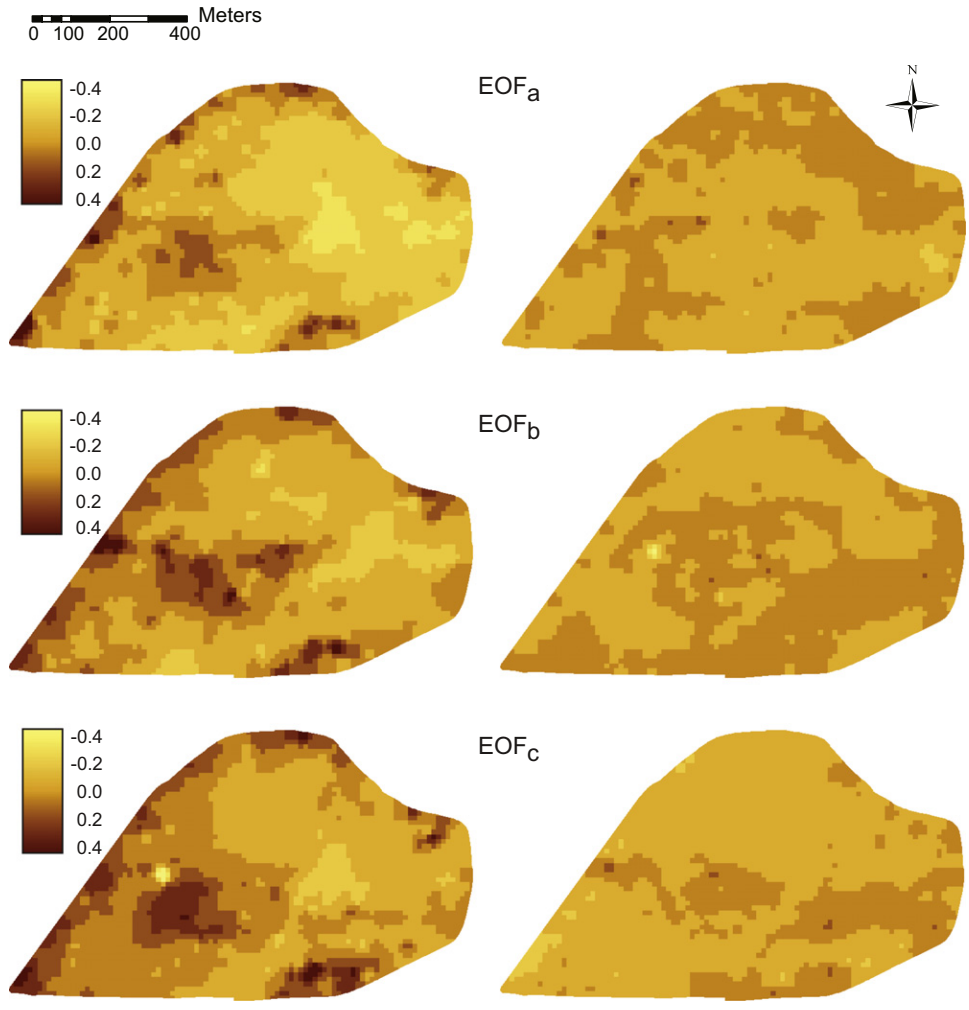


**Fig. 3.** The spatial pattern of soil water content as generated by the interpolated EOF1 (left three) and EOF2 (right three) from the three blocks of the CAF.

**Table 2**
Correlations between the EOFs of the spatial soil water anomalies and soil and topographic attributes.

| Attribute | Block A | | | | Block B | | | | Block C | | | |
|---|---|---|---|---|---|---|---|---|---|---|---|---|
| | EOF1 | EOF2 | EOF3 | EOF4 | EOF1 | EOF2 | EOF3 | EOF4 | EOF1 | EOF2 | EOF3 | EOF4 |
| Bulk density | 0.486 | 0.058 | 0.019 | −0.100 | 0.604 | 0.075 | 0.079 | 0.201 | 0.543 | 0.091 | 0.122 | −0.034 |
| Spring $EC_a$ | 0.589 | 0.191 | 0.214 | 0.170 | 0.676 | 0.358 | 0.103 | −0.197 | 0.643 | 0.406 | 0.122 | 0.089 |
| Elevation | −0.609 | −0.035 | −0.027 | 0.003 | −0.707 | −0.169 | −0.130 | 0.035 | −0.467 | 0.136 | 0.083 | 0.237 |
| Slope | −0.349 | −0.013 | 0.024 | 0.030 | −0.135 | 0.002 | −0.173 | 0.334 | −0.280 | 0.114 | 0.006 | 0.148 |
| Profile curvature | 0.465 | 0.299 | 0.080 | 0.008 | 0.486 | −0.046 | −0.073 | −0.018 | 0.375 | −0.158 | −0.051 | 0.038 |
| Flow accumulation | 0.182 | −0.082 | 0.035 | −0.054 | 0.425 | −0.078 | −0.030 | −0.243 | 0.253 | 0.146 | 0.024 | −0.248 |
| Wetness index | 0.386 | 0.180 | 0.051 | −0.094 | 0.474 | −0.069 | 0.031 | −0.032 | 0.398 | −0.156 | 0.066 | −0.189 |

larger in block B as compared to the A and C blocks, especially with EOF1 (Table 1). The spatial pattern across CAF as generated by the interpolated first two EOFs from the three blocks is shown in Fig. 3. The overall pattern based on EOF1 from the three blocks was similar, and consistent with the topography of the watershed. Large positive EOF1 values are mostly found at locations with lower elevation on the west and southeastern parts of the watershed (Fig. 3, left). These values represent locations with large positive soil water anomalies (i.e. wet locations), since all values of the first expansion coefficient (EC1) associated with EOF1 from all three blocks were positive values. On the other hand, locations with large negative EOF1 represent areas with negative soil water anomalies (i.e. dry locations), and are mostly found in higher elevation areas at the east side of the CAF. Despite the qualitative similarity in the spatial pattern of EOF1 among the three blocks, quantitative differences were observed especially with the EOF from block A. Using EOF1 from block A, about 32% of all locations at the CAF had relatively large negative EOF1 values (below −0.2), as compared to only 5% and 3% of locations when using EOF1 from the B and C blocks, respectively. Similar trend was also found with relatively large positive EOF1 values (above 0.2), with 1% of all locations based on EOF1 from block A found to have this category compared to 5% and 6% of locations when using EOF1 from the B and C blocks, respectively. Also blocks B and C had very close mean EOF1 values (0.04 and 0.05) across the entire CAF, and almost similar standard deviations, whereas block A had smaller mean EOF1 (−0.03), and larger standard deviation. These results show that more consistency is found between the B and C blocks, as will be more apparent from the following results.

The spatial pattern of EOF2 varied significantly between the three blocks, but values showed much less variability with smaller means and standard deviations as compared to EOF1 (Fig. 3, right). For the three blocks, EOF2 values were dominated by moderate positive and negative values (−0.1 to 0.1), this range covered about 98% of all locations in the three blocks. In block A, most of the positive EOF2 values were concentrated in the north and southwestern parts of the CAF, whereas for the C block the positive EOF2 were mostly concentrated in the southeastern part. Block B showed moderate positive EOF2 values distributed over most of the CAF (Fig. 3, right middle). The spatial pattern for the remaining EOF3 and EOF4 showed an inconsistent pattern among the three blocks (data not shown). However, these two EOFs were responsible for explaining about 5–13% of the total variation observed in soil water and consequently would have less importance in characterizing the spatial pattern of soil water dynamics at the CAF.

### 3.2. Role of topographic and soil properties

Correlation coefficient analysis showed that EOF1 had the highest correlation with elevation, especially in block B (−0.71) (Table 2). This high correlation is expected since, as discussed earlier, large EOF1 values are associated with lower elevation areas on the west and southeastern parts of the watershed. Similar findings were reported by Yoo and Kim (2004), who used EOF analysis to characterize spatio-temporal variability of soil water based on gravimetric soil water data from two agricultural field sites (SGP97, Little Washita ~0.64 $km^2$). They found that 70% of the observed soil water variability could be represented by a single

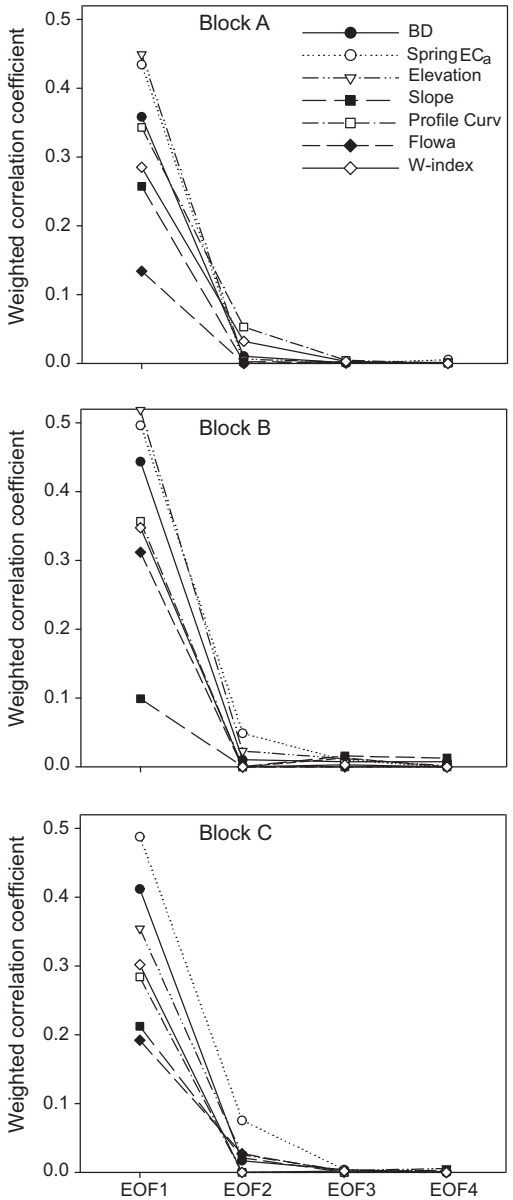


**Fig. 4.** Weighted correlation coefficients between EOF1 generated from the three blocks A, B, and C and soil and topographic attributes.

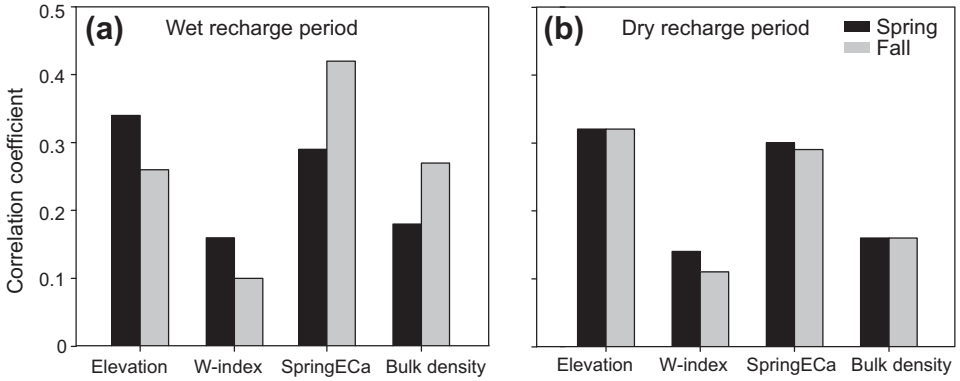


**Fig. 5.** Average correlation coefficients between estimated soil water and soil and topographic attributes during spring and fall of (a) years of wet recharge period (September–April) (2002, 2003, 2004, 2006) (average of 44.36 cm), and (b) years of dry recharge period (2001, 2005) (average of 26.31 cm) in the CAF.

spatial soil water pattern that was correlated with topographic attributes. Nonetheless, they pointed out that soil water evolution is a complex process and that other factors like soil properties and land use are also important factors, particularly after precipitation events conclude. High correlations were also found with both bulk density and spring $EC_a$ readings, with average correlations among the three blocks of 0.64 and 0.55 for the $EC_a$ and the bulk density, respectively. Other topographic attributes showed moderate correlations, with average correlations among the three blocks of 0.44, 0.42, 0.28 and −0.26 for the profile curvature, wetness index, flow accumulation, and slope, respectively. Weighted pattern correlations with EOF1 showed that the previously discussed ranking of correlation coefficients is consistent for A and B blocks (Fig. 4). In block C the order is slightly different with soil properties showing slightly higher correlations than elevation. Weighted pattern correlations also showed that in general, EOF1 generated from block B showed higher correlations with soil and topographic properties, followed by EOF1 generated from the C and A blocks.

EOF2 had smaller correlation coefficients with soil and topographic attributes in the three blocks (Table 2). The only exception was with spring $EC_a$ readings in the B and C blocks, with correlations of 0.36 and 0.41, respectively. The higher order EOFs had very low correlations with all soil and topographic attributes, especially when being weighted by the smaller amount of variance they explain (Fig. 4).

### 3.3. Spatial patterns of soil water

Due to the fact that the first EOF/EC pair explained about 73–76%, and that the first two EOF/EC pairs explained together about 87–95% of variability in the three blocks, we used only the first two EOF/EC pairs to estimate soil water at the CAF. Topographic properties were the most important factors dominating soil water patterns followed by spring $EC_a$ and bulk density. This is expected since the first EOF used to estimate the soil water pattern was found to be highly correlated with both elevation and wetness index in the CAF (Table 1). However, this relationship varies between spring and fall especially in the years 2002, 2003, 2004, and 2006 where larger amounts of precipitation were received (yearly average of 44.36 cm). More variability was observed between the spatial patterns of soil water during spring and fall of these years. Because of the larger amount of rain received in these years, wet conditions are observed over many locations, and the role of topographic attributes become more important in determining the soil water patterns. This is evident by the close resemblance, and the larger correlation coefficients, between the soil water patterns in the spring and the spatial distribution of elevation ($r^2 = 0.34$) and wetness index ($r^2 = 0.16$) of the CAF. $EC_a$ and bulk density played the second important role with correlation coefficients with the estimated soil water of 0.29 and 0.18, respectively (Fig. 5a). As the soil profile dries out during fall, the role of topographic attributes starts to diminish and soil properties become more important in determining the soil water patterns. The soil water patterns during fall of these years resemble the pattern of distribution of $EC_a$ ($r^2 = 0.42$) and bulk density ($r^2 = 0.27$) values generated over the entire CAF. During fall, correlation coefficients between soil water and elevation and wetness index were 0.26 and 0.10, respectively (Fig. 5a). Yoo and Kim (2004) reported that topographic attributes were highly correlated with the EOFs generated from two field sites at the (SGP97) little Washita, and they dominated the spatial pattern of soil water during rainfall and wet periods. They found that after rainfall stops, the role of topographic attributes becomes less important and soil and land use properties become more important in controlling soil water variability. Because less precipitation was received during 2001 and 2005 (yearly average of 26.31 cm), less variability was observed in the soil water patterns between the spring and fall during these years as indicated by the very close correlation coefficients between soil water and topographic and soil properties during spring and fall (Fig. 5b).

Based on the performance of the interpolated EOFs in estimating soil water content during the years 1999–2000, EOFs from the B and C blocks showed more consistent estimates of soil water as compared to soil water estimated from the A block (Fig. 6). Interpolated EOFs from the B and C blocks gave very close estimates of soil water content over the entire CAF when the first two EOF/EC pairs were included in the estimation. Average water content in both the B and C blocks was 0.55 and 0.31 m profile$^{-1}$ during spring and fall of 1999–2000, respectively. In contrast, the first two EOF/EC pairs interpolated from block A gave an average water content of 0.49 and 0.26 m profile$^{-1}$ during spring and fall of 1999–2000, respectively. Correlation coefficients between measured and estimated soil water content were larger with estimates based on EOFs interpolated from the B block (Fig. 6), followed by estimates from the C and A blocks. These results indicate that EOFs interpolated from both the B and C blocks provided better estimate of soil water, and can be used interchangeably to represent the entire CAF. Jawson and Niemann (2007) examined the effect of the areal extent of a region on the pattern of the generated EOFs by dividing the SGP97 field campaign area into northern and southern sub-regions, and comparing the EOFs generated from each sub-region separately to those generated from the entire area. The EOF patterns obtained from the two sub-regions were very similar to those obtained from the entire area. They explained that this would be the case when there is no significant difference between the spatial average soil water in the two sub-regions. The spatial

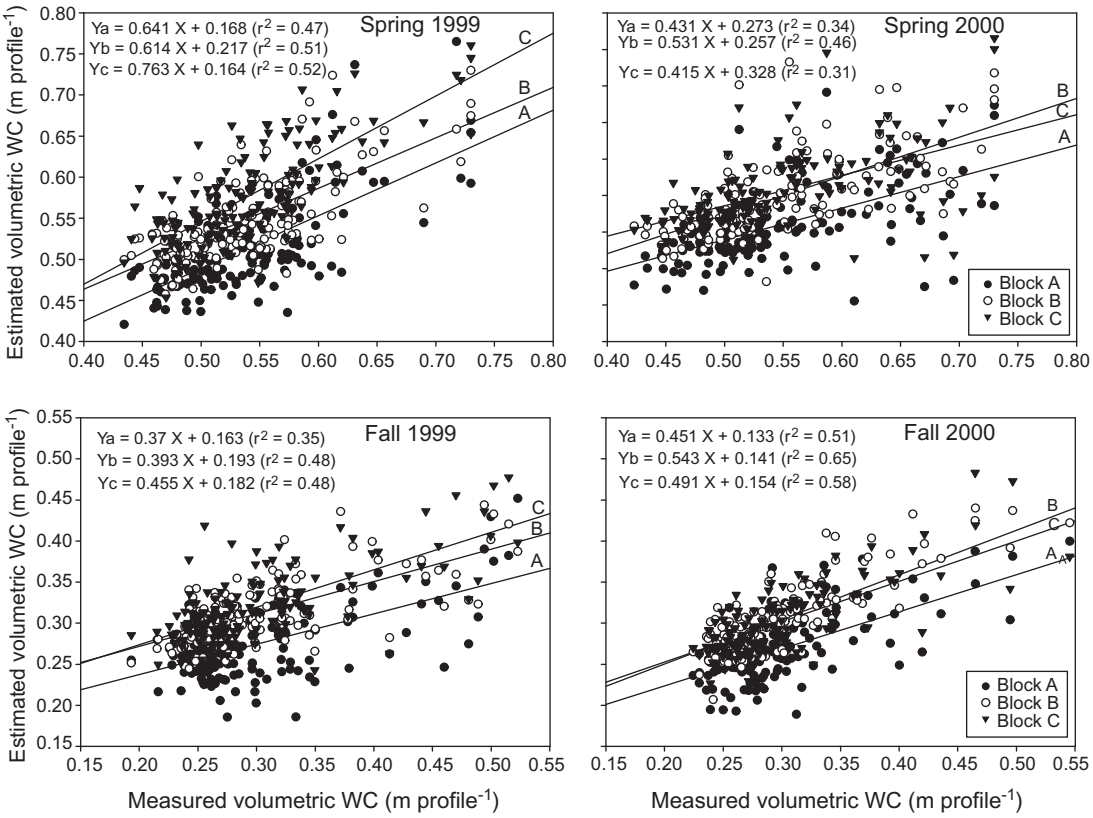


**Fig. 6.** Correlation coefficients between measured and estimated soil water content (m profile$^{-1}$) using the first two EOF/EC pairs interpolated from the three blocks of the CAF during spring and fall of 1999–2000 (note variable units on axes).

average soil water is usually very similar in the three blocks of the CAF (the range for the years 2001–2006 was 0.49–0.54 and 0.29–0.31 m profile$^{-1}$ during spring and fall, respectively), which explains the similarity of the EOFs patterns generated from the different blocks, especially with the first two EOFs, which explains large amount of the soil water variability in the CAF.

The accuracy of the soil water estimate as indicated by the NSCE varies significantly among the three blocks, with estimates from block B giving the best performance (Fig. 7). Using the average soil water, at any specific time, as an estimate of soil water at any location during this time will produce an NSCE value of zero. Both the A and C blocks include negative NSCE at several years indicating the estimate based on EOF interpolation from these blocks is performing worse than using the average soil water, which is assumed to be known, in these years. Only estimates based on EOF interpolation from the B block produced NSCE values greater than zero (min. is 0.1) during spring and fall of the years 2001–2006 (Fig. 7). These results suggest that despite the consistency between blocks B and C in producing similar spatial patterns of the soil water estimate over the entire watershed, estimates based on block B provided a more accurate estimate of soil water over the entire watershed when the estimation error was evaluated against measurements of soil water. When additional EOF/EC pairs were included into the process of soil water estimation, NSCE values either decreased or did not significantly increase beyond the value based on the first two EOF/EC pairs. The higher order EOF/EC pairs are usually associated with random spatial variation, and as a result will likely cause an increase in the estimation error when included (Perry and Niemann, 2008).

The performance of the EOF interpolation method to estimate soil water gave the best results with EOF/EC pairs generated from the B block, with average NSCE values of 0.47 as compared to average NSCE values of 0.23 and 0.01 with EOF/EC pairs generated from the C and A blocks, respectively. The maximum average NSCE values over the 6 years period from 2001 to 2006 were observed using EOF from the B block when only the first two EOF/EC pairs were included, with an average of 0.49 and 0.44 during fall and spring, respectively. Despite this slight increase in the average NSCE values during fall based on EOF from the B block, the estimation methods worked in general slightly better during spring with an overall average NSCE from all three blocks of 0.23 as compared to 0.20 during fall over the entire watershed. Similar findings were found by Perry and Niemann (2007), who reported that estimating soil water based on EOF and other interpolation methods

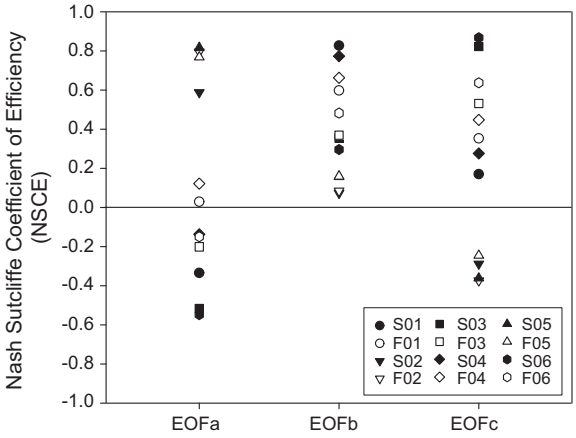


**Fig. 7.** NSCE of the total soil water content as estimated by the first two EOF/EC pairs from the three blocks of the Cook Agronomy Farm. Different symbols represent values during spring and fall of the years 2001–2006.

performed better for wet as compared to dry periods when soil water variability is usually smaller.

### 3.4. EOF-based soil water estimation

Soil water contents were estimated for the years 2001–2006 using the interpolated EOFs generated from block B. The average NSCE value over the 6 years was 0.48. The highest NSCE values were obtained with the years 2001 and 2004 (average of 0.87), followed by the years 2003 and 2006 (average of 0.42). The 2 years 2002 and 2005 gave the lowest NSCE values (average of 0.15). Since the interpolated EOF1 and EOF2 used in the estimation were generated from Block B, the error associated with extrapolating the generated EOFs to blocks A and C led to smaller NSCE values, especially in the years 2002 and 2005 (Fig. 7). Correlation coefficient analysis between measured and estimated soil water showed similar results (Figs. 8 and 9). The largest correlation coefficients were obtained during spring and fall of 2001 and reached 0.82 and 0.83, respectively (Figs. 8 and 9). The average correlation coefficient over the 6 years was 0.54, and the average for the years 2001/2004, 2002/2005, and 2003/2006 was 0.76, 0.40, and 0.48, respectively. The large NSCE and correlation coefficients values obtained between measured and estimated water content suggest that the EOF-based method to estimate soil water can effectively predict soil water content at the CAF. Perry and Niemann (2008) attributed the better performance of the EOF interpolation method to the fact that it uses information of soil water from several measurement times (four in our case) to identify the spatial pattern of soil water, which is used later to estimate soil water at other times. This provides a better estimate then regression methods (e.g. SMLR), which estimates soil water based on information from a single measurement time.

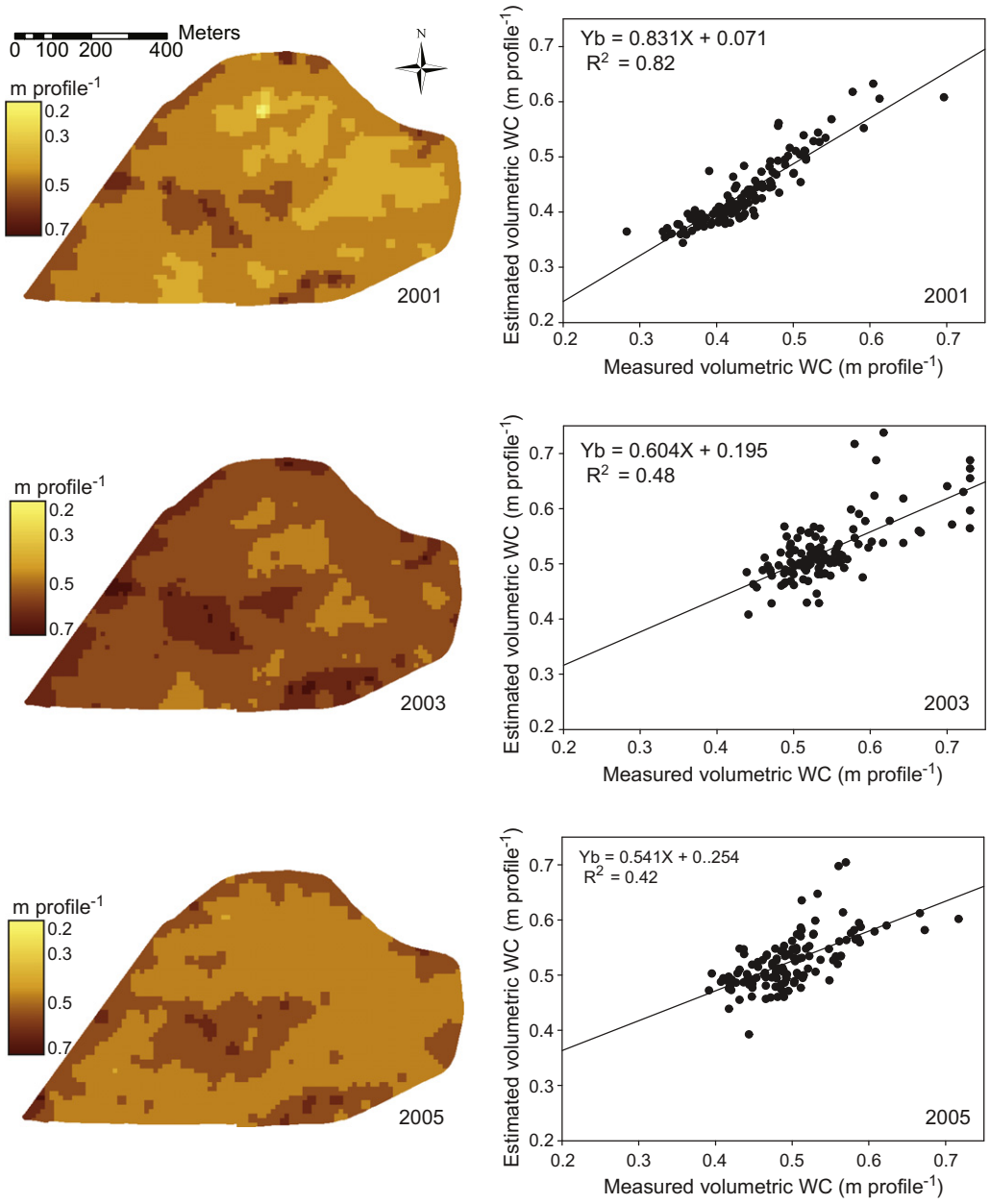


**Fig. 8.** Soil water content (m profile$^{-1}$) as estimated by the first two EOF/EC pairs interpolated from block B of the CAF during spring of 2001, 2003, and 2005 (left three), and correlation coefficients between measured and estimated soil water (right three).

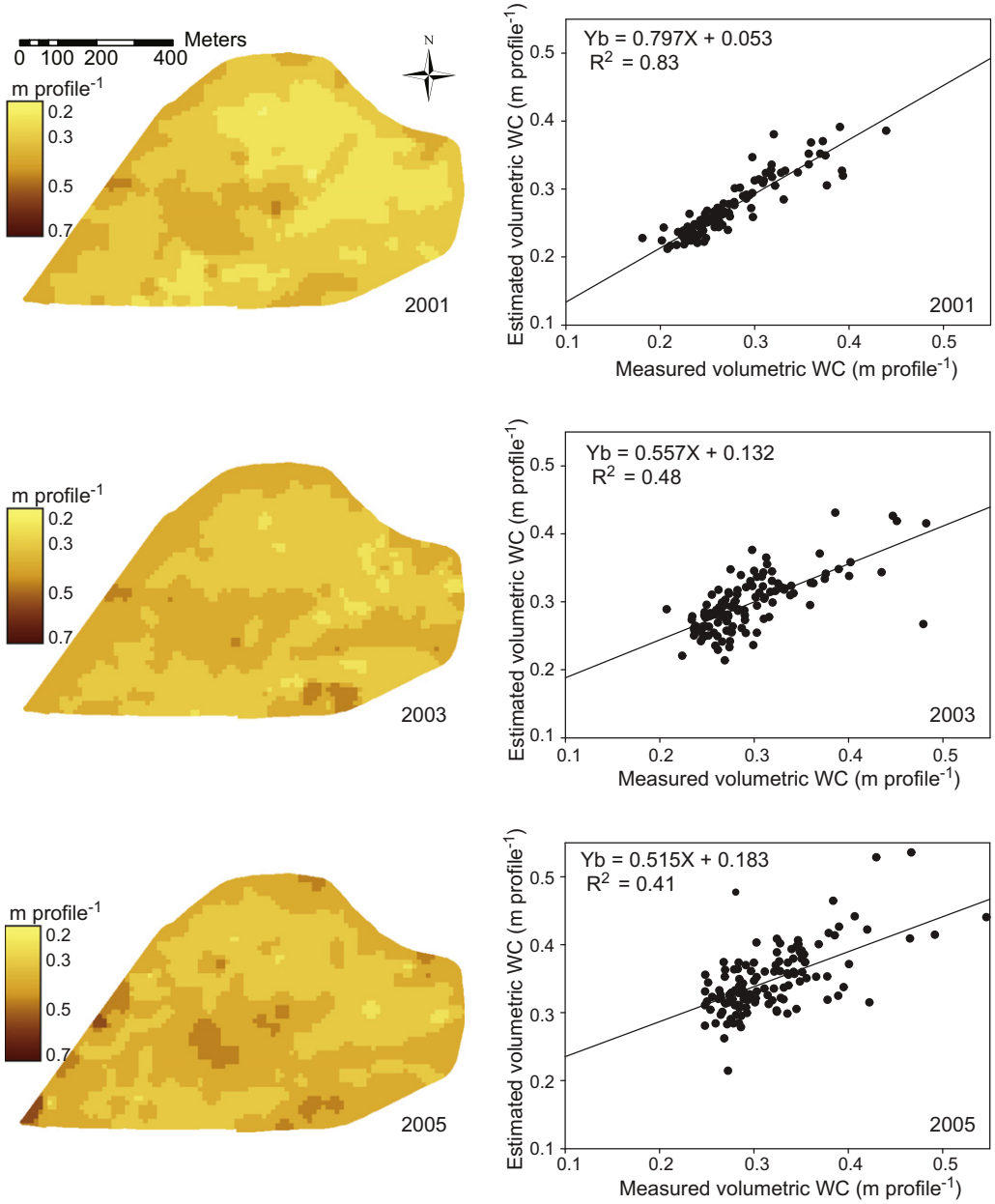


**Fig. 9.** Soil water content (m profile$^{-1}$) as estimated by the first two EOF/EC pairs interpolated from block B of the CAF during fall of 2001, 2003, and 2005 (left three), and correlation coefficients between measured and estimated soil water (right three).

## 4. Summary and conclusion

In this study, we used EOF analysis to examine the spatial patterns of soil water variability at the CAF near Pullman, Washington. The EOFs were generated from the spatial anomalies of the soil water measurements collected from one of the three blocks (A, B, and C) of the farm during the years 2001–2006. The generated EOFs were interpolated, using topographic and soil attributes collected at the same measurement locations, and used to estimate soil water variability summed over the top 1.5 m. The spatial patterns of soil water also were correlated with topographic and soil properties to identify controlling factors and how they affect the dynamics of soil water. The first EOF generated from the three blocks of the CAF explained about 73–76% of the soil water variability, which indicates the existence of a common factor dominating the spatial pattern of soil water variation within the watershed. EOF1 generated from block B and C were more consistent (closer means and standard deviations), as compared to EOF1 generated from block A. In general, the first EOF had the highest correlation coefficient with topographic attributes, especially with elevation in block B (−0.71). The next higher correlations were observed with spring $EC_a$ and bulk density. EOF2 had smaller correlations with topographic attributes and soil properties, and only $EC_a$ showed moderate correlations in blocks B and C (0.36 and 0.41). Higher order EOFs showed very small correlations with both topographic attributes and soil properties. Soil water patterns based on EOF interpolation varied between wet and dry conditions during spring and fall seasons. Under wet conditions, elevation and wetness index were the main factors regulating the spatial patterns of soil water as evident by the similarity of the soil water pattern and the distribution pattern of these attributes, and larger correlation coefficients with the estimated soil water. Spring estimates of

soil water storage are particularly important in this dryland farming region as stored soil water is a major determinant of potential wheat grain yield. Furthermore, predictable patterns of stored soil water in the spring can serve as the basis for delineating precision management zones. As the soil dries out during the summer, soil properties (spring $EC_a$ and bulk density) became more important in controlling the spatial patterns of soil water.

More consistent soil water estimates over the entire CAF were obtained by interpolating the EOFs generated from blocks B and C. However, EOFs generated from block B provided larger NSCE values and more accurate estimate of soil water, especially when the first two EOF/EC pairs were retained. Including more than the first two EOF/EC pairs did not significantly increase the NSCE of soil water estimate, and in some cases even produced lower NSCE values. The EOF interpolation method to estimate soil water variability worked slightly better during spring than during fall, with average NSCE values of 0.23 and 0.20, respectively. The less soil water variability usually occurring during summer and fall would explain the larger NSCE values of soil water observed during spring. In general, the EOF interpolation method to estimate soil water variability has two main advantages over other regression methods: (1) it estimates the soil water variability based on soil water data from several measurement times, whereas in the case of other regression methods (e.g. SMLR) only soil water measurement at one single time is used. (2) The analysis is simple and requires much less data than most multiple regression methods, which require the collection of large amount of topographic and soil data at measurement locations. Also the higher correlation observed between the EOFs and topographic and soil attributes suggests that using the generated EOFs in the regression against topographic and soil properties would be advantageous to using direct soil water measurements.

## References


Bardossy, A., Lehmann, W., 1998. Spatial distribution of soil moisture in a small catchment. Part 1: geostatistical analysis. J. Hydrol. 206, 1–15.

Beven, K.J., Kirkby, M.J., 1979. A physical based, variable contributing area model of basin hydrology. Hydrol. Sci. 24, 43–69.

Burt, T.P., Butcher, D.P., 1985. Topographic controls of soil moisture distributions. J. Soil Sci. 36, 469–486.

Busacca, A.J., Montgomery, J.A., 1992. Field-landscape variation in soil physical properties of the Northwest dryland crop production region. In: Veseth, R., Miller, B. (Eds.), Precision Farming for Profit and Conservation. 10th Inland Northwest Conservation Farming Conference Proceedings. Washington State University, Pullman.

Cosh, M.H., Stedinger, J.R., Brutsaert, W., 2004. Variability of surface moisture at the watershed scale. Water Resour. Res. 40, W12513. doi:10.1029/2004WR003487.

Crave, A., Gascuel-Odoux, C., 1997. The influence of topography on time and space distribution of soil surface water content. Hydrol. Process. 11, 203–210.

Deutsch, C.V., Journel, A.G., 1992. GSLIB, Geostatistical Software Library and User's Guide. Oxford University Press, New York, New York.

Famigliett, J.S., Rudnicki, J.W., Rodell, M., 1998. Variability in surface moisture content along a hillslope transect: Rattlesnake Hill, Texas. J. Hydrol. 210, 259–281.

Fiez, T.E., Pan, W.L., Miller, B.C., 1995. Nitrogen efficiency analysis of winter wheat among landscape positions. Soil Sci. Soc. Am. J. 59, 1666–1671.

Florinsky, I.V., Eilers, R.G., Manning, G.R., Fuller, L.G., 2002. Prediction of soil properties by digital terrain modeling. Environ. Modell. Softw. 17, 295–311.

Limited, Geonics., 2000. Geonics EM 38 Ground Conductivity Meter Operating Manual. Geonics Ltd., Mississauga, Ont., Canada.

Green, T.R., Erskine, R.H., 2004. Measurement, scaling, and topographic analyses of spatial crop yield and soil water content. Hydrol. Process. 18, 1447–1465.

Hu, Z., Chen, Y., Islam, S., 1998. Multiscaling properties of soil moisture images decomposition of large- and small-scale features using wavelet transforms. Int. J. Remote Sensing 19 (13), 2451–2467.

Hupet, F., Vanclooster, M., 2002. Intraseasonal dynamics of soil moisture variability within a small agricultural maize cropped field. J. Hydrol. 261, 86–101.

Jaynes, D.B., Kaspar, T.C., Colvin, T.S., James, D.E., 2003. Cluster analysis of spatiotemporal corn yield patterns in an Iowa field. Agron. J. 95, 574–586.

Jackson, T.J., Le Vine, D.E., 1996. Mapping surface soil moisture using an aircraft-based passive microwave instrument: algorithm and example. J. Hydrol. 184, 85–99.

Jawson, S.D., Niemann, J.D., 2007. Spatial patterns from EOF analysis of soil moisture at a large scale and their dependence on soil, land-use, and topographic properties. Adv. Water Resour. 30, 366–381.

Kim, C.P., Stricker, J.N.M., 1996. Influence of spatially variable soil hydraulic properties and rainfall intensity on the water budget. Water Resour. Res. 32 (6), 1699–1712.

Kim, G., Barros, A.P., 2002. Downscaling of remotrly sensed soil moisture with modified fractal interpolation method using contraction mapping and ancillary data. Remote Sens. Environ. 83, 400–413.

Mallawatantri, A.P., McConkey, B.G., Mulla, D.J., 1996. Characterization of pesticide sorption and degradation in macropore linings and soil horizons of Thatuna silt loam. J. Environ. Qual. 25, 227–235.

Nash, J.E., Sutcliffe, J.V., 1970. River forecasting through conceptual models, part I, a discussion of principle. J. Hydrol. 10, 282–290.

North, G.R., Bell, T.L., Cahalan, R.F., Moeng, F.J., 1982. Sampling errors in the estimation of empirical orthogonal functions. Mon. Weather Rev. 110, 699–706.

Nyberg, L., 1996. Spatial variability of soil water content in the covered catchment at Gardsjon, Sweden. Hydrol. Process. 10, 89–103.

Pan, W.L., Hopkins, A.G., 1991. Plant development, and N and P use of winter barley. I. Evidence of water stress-induced P deficiency in an eroded toposequence. Plant Soil 135, 9–19.

Pan, W.L., Schillinger, W., Huggins, D.R., Koenig, R., Burns, J., 2007. Fifty years of predictingwheat nitrogen requirements in the Pacific Northwest USA. Managing crop nitrogen for weather. In: Bruulsema, T.W. (Ed.), Proceedings of the Soil Science Society of America Symposium on Integrating Water Variability into Nitrogen Recommendations, 15 November 2006, Indianapolis, IN. International Plant Nutrition Institute, Norcross, GA, USA.

Perry, M.A., Niemann, J.D., 2007. Analysis and estimation of soil moisture at the catchment scale using EOFs. J. Hydrol. 334, 388–404.

Perry, M.A., Niemann, J.D., 2008. Generation of soil moisture patterns at the catchment scale by EOF interpolation. Hydrol. Earth Syst. Sci. 12, 39–53.

Pietroniro, A., Prowse, T.D., 2002. Applications of remote sensing in hydrology. Hydrol. Process. 16, 1537–1541.

Preisendorfer, R.W., 1988. Principal Component Analysis in Meteorology and Oceanography. Development of Atmospheric Science, vol. 17. Elsevier, pp. 425.

StarPal, 1997. HGIS, GPS Mapping Software for Windows, StarPal Inc., 2531 Wapiti Road, Fort Collins, CO 80525, USA.

Sudduth, K.A., Drummond, S.T., Kitchen, N.R., 2001. Accuracy issues in electromagnetic induction sensing of soil electrical conductivity for precision agriculture. Comput. Electr. Agr. 31, 239–264.

Thattai, D., Islam, S., 2000. Spatial analysis of remotely sensed soil moisture data. J. Hydrol. Eng. 5, 386–392.

Trimble Navigation, 2001. TSC1 Asset Surveyor Software User Guide. Trimble Navigation Limited.

Uberuaga, D. 2004. Resolution of Digital Elevation Models and Terrain Attributes, Apparent Electrical Conductivity, and Prediction of Palouse Soilscape Bt Horizons. MS. Thesis, Washington State University, Pullman, WA.

Ulaby, F.T., Dubois, P.C., van Zyl, J., 1996. Radar mapping of surface soil moisture. J. Hydrol. 184, 57–84.

Western, A.W., Grayson, R.B., 1998. The Tarrawarra data set: soil moisture patterns, soil characteristics, and hydrological flux measurements. Water Resour. Res 34 (10), 2765–2768.

Western, A.W., Bloschl, G., Grayson, R.B., 1998. Geostatistical characterization of soil moisture patterns in Tarrawarra catchment. J. Hydrol. 205, 20–37.

Western, A., Grayson, R., Green, T., 1999a. The Tarrawarra project: high resolution spatial measurement, modeling and analysis of soil moisture and hydrologic response. Hydrol. Process. 13, 633–652.

Western, A.W., Grayson, R.B., Bloschl, G., Willgoose, G.R., Mcmahon, T.A., 1999b. Observed spatial organization of soil moisture and its relation to terrain indices. Water Resour. Res. 35 (3), 797–810.

Western, A.W., Grayson, R.B., Bloschl, G., Wilson, D.J., 2003. Spatial variability of soil moisture and its implication for scaling. In: Perchepsky, Y.A., Radcliffe, D.E., Selim, H.M. (Eds.), Scaling Methods in Soil Physics. CRC Press, Boca Raton, FL, pp. 119–142.

Williams, A.G., Ternan, J.L., Fitzjohn, C., de Alba, S., Perez-Gonzalez, A., 2003. Soil moisture variability and land use in a seasonally arid environment. Hydrol. Process. 17, 225–235.

Wilson, D.J., Western, A.W., Grayson, R.B., Berg, A.A., Lear, M.S., Rodell, M., Famiglietti, J.S., Woods, R.A., McMahon, T.A., 2003. Spatial distribution of soil moisture over 6 and 30 cm depth, Mahurangi river catchment, New Zealand. J. Hydrol. 276, 254–274.

Wilson, D.J., Western, A.W., Grayson, R.B., 2005. A terrain and data-based method for generating the spatial distribution of soil moisture. Adv. Water Resour. 28, 43–54.

Wood, E.F., 1997. Effects of soil moisture aggregation on surface evaporative fluxes. J. Hydrol. 190, 397–412.

Yoo, C., Kim, S., 2004. EOF analysis of surface soil moisture field variability. Adv. Water Res. 27, 831–842.

Yoo, C., Valdes, J.B., North, G.R., 1998. Evaluation of the impact of rainfall on soil moisture variability. Adv. Water Res. 21, 375–384.

Yoo, C., Kim, S.J., Lee, J., 2001. Land cover change and its impact on soil-moisture-field evolution. J. Hydrol. Eng. 6 (5), 436–441.